

Measurements of global and local polarization of hyperons in isobar collisions at 200 GeV from STAR

Xingrui Gou^{1,*}, for the STAR Collaboration

¹Institute of Frontier and Interdisciplinary Science & Key Laboratory of Particle Physics and Particle Irradiation (Ministry of Education), Shandong University, Qingdao, Shandong, 266237, China

Abstract. In heavy-ion collisions, the observation of the global and local polarization of hyperons has revealed the existence of large vorticities perpendicular to reaction plane due to system's orbital angular momentum and along beam direction due to collective velocity field, respectively. With the high-statistics data from isobar collisions of Ru+Ru and Zr+Zr at $\sqrt{s_{NN}} = 200$ GeV collected by the STAR experiment, we present differential measurements of global polarization for $\Lambda/\bar{\Lambda}$ as a function of centrality. These measurements allow us to study the possible magnetic field driven effects through the polarization difference between Ru+Ru and Zr+Zr, owing to a larger magnetic field in the former. Furthermore, the first measurements of Λ hyperon local polarization along beam direction relative to the third-order event plane as well as the second-order event plane are presented. A comparison of results from isobar and Au+Au collisions provides important new insights into the collision system size dependence of the vorticities in heavy-ion collisions.

1 Introduction

In non-central heavy-ion collisions, the produced system has large orbital angular momentum and may have a strong vortical structure, which leads to the global spin polarization of hyperons through the spin-orbital interaction [1]. Due to the nature of the weak decay, Λ hyperon's polarization can be determined through the angular distribution of decay daughter proton in parent's rest frame.

Global polarization has been observed for Λ and $\bar{\Lambda}$ hyperons in Au+Au collisions from $\sqrt{s_{NN}} = 7.7$ to 200 GeV by the STAR experiment [2, 4]. Significant global polarization of $\Lambda(\bar{\Lambda})$ observed from low to high energy is consistent with the expectation from the spin-orbit coupling picture, which can be described by hydrodynamic models. Some models predict a system size dependence of global polarization [3, 5]. Experimentally, the system size dependence can be studied by comparing results in isobar collisions with those in Au+Au collisions. Furthermore, the magnetic field effects may cause a splitting between Λ and $\bar{\Lambda}$ global polarization, and initial magnetic field difference between Ru+Ru and Zr+Zr collision may lead to different Λ global polarization in the two systems.

On the other hand, STAR has measured the local polarization with respect to the second-order event plane in Au+Au collisions at $\sqrt{s_{NN}} = 200$ GeV [7]. The local polarization as a function of azimuthal angle relative to the second-order event plane shows a sine modulation,

*e-mail: xgou@rcf.thic.bnl.gov;xingruigou@mail.sdu.edu.cn

38 as expected from quadrupole structure of vorticity along the beam direction. With high statistics isobar data, measurements of local polarization in smaller systems and relative to higher
 39 harmonics event planes can provide new insights into polarization phenomena.
 40

41 In these proceedings, we report $\Lambda(\bar{\Lambda})$ global and local polarization as a function of centrality in Ru+Ru and Zr+Zr collisions at $\sqrt{s_{NN}} = 200$ GeV using the data collected by STAR
 42 experiment.
 43

44 2 Global polarization results

In STAR experiment, the first-order event plane can be determined by Zero Degree Calorimeters with Shower Maximum Detectors (ZDC SMD), the second-order and third-order event planes are determined by Time Projection Chamber detector (TPC). $\Lambda(\bar{\Lambda})$ hyperons have been reconstructed through its decay channel: $\Lambda \rightarrow \pi^- + p$ ($\bar{\Lambda} \rightarrow \pi^+ + \bar{p}$). The residual background under mass peak is smaller than 3%. The global polarization is determined by

$$P_{\Lambda} = \frac{8}{\alpha\pi} \frac{1}{A^0} \frac{\langle \sin(\Psi_1 - \phi_p^*) \rangle}{\text{Res}(\Psi_1)}, \quad (1)$$

45 where α is decay parameter, A^0 is acceptance correction factor, ϕ_p^* is the azimuthal angle of decay proton in Λ 's rest frame and $\text{Res}(\Psi_1)$ is the first-order event plane resolution [2].

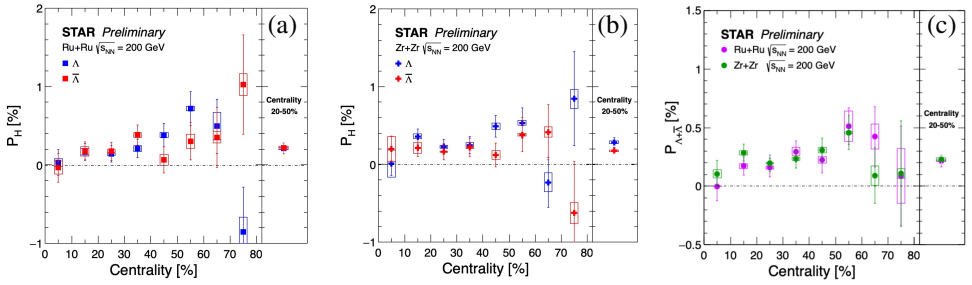


Figure 1: Global polarization of Λ and $\bar{\Lambda}$ as a function of centrality in Ru+Ru(a), Zr+Zr(b) collisions at $\sqrt{s_{NN}} = 200$ GeV. Panel (c) shows $\Lambda + \bar{\Lambda}$ global polarization results in isobar collisions. Open boxes and vertical lines represent systematic and statistical uncertainties.

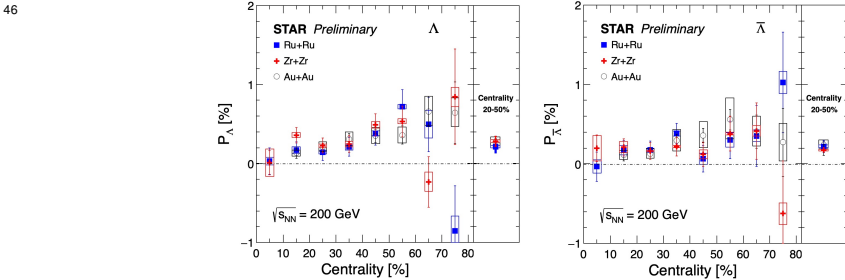


Figure 2: Λ (left) and $\bar{\Lambda}$ (right) global polarization as a function of centrality in Ru+Ru, Zr+Zr, and Au+Au collisions at $\sqrt{s_{NN}} = 200$ GeV.

47 Figure 1 (a) and (b) show Λ and $\bar{\Lambda}$ global polarization $P_{\Lambda/\bar{\Lambda}}$ as a function of centrality
 48 in Ru+Ru and Zr+Zr collisions. The results increase from central to peripheral centrality.

49 For better precision, we also combine 20-50% centrality results. No significant difference
 50 between Λ and $\bar{\Lambda}$ global polarization in Ru+Ru and Zr+Zr collisions has been observed
 51 which indicates that no magnetic field effects on the hyperon polarization is observed in
 52 isobar collisions within current statistical limitation.

53 Figure 1 (right) shows $\Lambda + \bar{\Lambda}$ global polarization $P_{\Lambda + \bar{\Lambda}}$ as a function of centrality in Ru+Ru
 54 and Zr+Zr collisions. The results are consistent in each centrality between Ru+Ru and Zr+Zr
 55 collisions.

56 Figure 2 shows Λ and $\bar{\Lambda}$ global polarization comparison between isobar and Au+Au
 57 collisions. The results are consistent between isobar and Au+Au collisions for the whole
 58 centrality range, indicating there is little collision system size dependence.

59 3 Local polarization results

The component of the polarization along the beam direction can be measured by

$$\langle \cos\theta_p^* \rangle = \int \frac{dN}{d\Omega^*} \cos\theta_p^* d\Omega^*, \quad (2)$$

60 where θ_p^* is the polar angle of the daughter proton in the Λ rest frame [7].

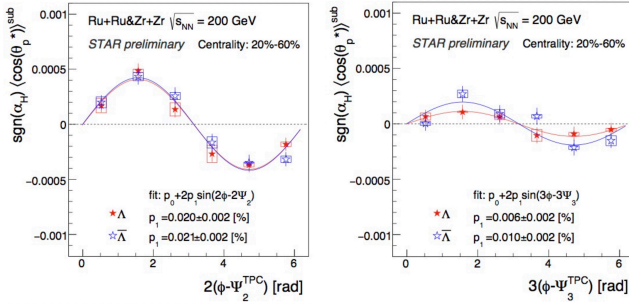


Figure 3: $\langle \cos\theta_p^* \rangle$ of Λ and $\bar{\Lambda}$ hyperons as a function of azimuthal angle ϕ relative to the second-order event plane Ψ_2 (left) and third-order event plane Ψ_3 (right) for 20% – 60% centrality in isobar collisions at $\sqrt{s_{NN}} = 200$ GeV. $\langle \rangle^{sub}$ denotes the subtraction of the acceptance effect. Solid lines show the fit with the sine function.

61 Figure 3 shows $\langle \cos\theta_p^* \rangle$ of Λ and $\bar{\Lambda}$ hyperons as a function of azimuthal angle ϕ relative
 62 to the second-order event plane Ψ_2 (left) and third-order event plane Ψ_3 (right) for 20% – 60%
 63 centrality respectively. The solid lines are the fits to the results with $p_0 + 2p_1 \sin(n\phi - n\Psi_n)$.
 64 The signal on Figure 3 (left) shows a clear sine modulation, as expected from quadrupole
 65 structure of vorticity along the beam direction. The trend is similar to that in Au+Au collisions.
 66 Figure 3 (right) shows the first measurements of $\langle \cos\theta_p^* \rangle$ with respect to the third-order
 67 event plane Ψ_3 . The results also show a sine modulation for both Λ and $\bar{\Lambda}$, indicating a v_3
 68 driven polarization.

69 Figure 4 (left) presents the centrality dependence of the second and third Fourier sine
 70 coefficients of the local polarization $\langle P_z \sin[n(\phi - \Psi_n)] \rangle$. The increase of the results with
 71 centrality is in line with the increasing of elliptic flow magnitude towards peripheral collisions.
 72 A significant local polarization with respect to the third-order event plane has been
 73 observed which increases with centrality. The results show no significant difference between
 74 the second-order and third-order local polarization within uncertainties. The hydrodynamic
 75 model with a shear term [6] reasonably describes the data for central collisions, but not for
 76 the peripheral ones.

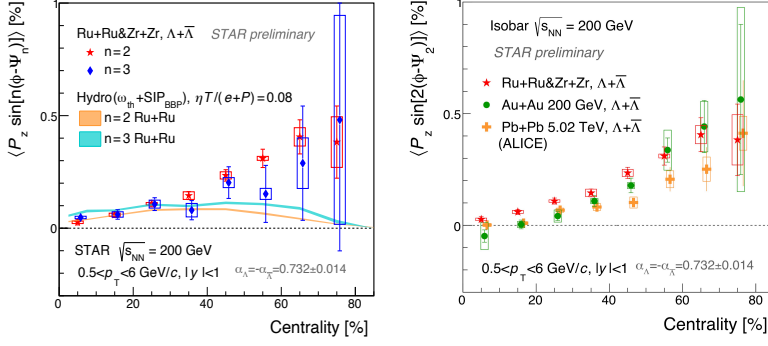


Figure 4: Left: the second and third Fourier sine coefficients of the local polarization of $\Lambda + \bar{\Lambda}$ as a function of the collision centrality in isobar collisions at $\sqrt{s_{NN}} = 200$ GeV. Right: the comparison of the second Fourier sine coefficient of $\Lambda + \bar{\Lambda}$ local polarization among isobar, Au+Au collisions at $\sqrt{s_{NN}} = 200$ GeV and Pb+Pb collisions at $\sqrt{s_{NN}} = 5.02$ TeV.

77 Figure 4 (right) shows the $\langle P_z \sin [2(\phi - \Psi_2)] \rangle$ of $\Lambda + \bar{\Lambda}$ local polarization with respect to
78 the second-order event plane as a function of the collision centrality in isobar, Au+Au, and
79 Pb+Pb collisions [8]. A hint of system size dependence has been observed comparing isobar
80 and Au+Au collisions at $\sqrt{s_{NN}} = 200$ GeV, while the energy dependence is not obvious
81 between $\sqrt{s_{NN}} = 200$ GeV Au+Au collisions and $\sqrt{s_{NN}} = 5.02$ TeV Pb+Pb collisions.

82 4 Summary

83 The global and local polarizations of Λ and $\bar{\Lambda}$ have been measured in Ru+Ru and Zr+Zr
84 collisions at $\sqrt{s_{NN}} = 200$ GeV. For global polarization, Λ and $\bar{\Lambda}$ results are consistent, showing
85 that the magnetic field effects on global polarization are not observed in isobar collisions
86 within current statistical limitation. Global polarization results are consistent between
87 Ru+Ru, Zr+Zr, and Au+Au collisions. No obvious collision system size dependence is observed.
88 Significant local polarization signals with respect to the second-order and third-order
89 event plane are observed in isobar collisions at $\sqrt{s_{NN}} = 200$ GeV. A hint of collision system
90 size dependence has been observed, while energy dependence is not obvious.

91 Acknowledgements

92 The author is supported partially by the National Natural Science Foundation of China
93 under No.11890710, No.11890713.

94 References

- 95 [1] Z. T. Liang and X. N. Wang, Phys. Rev. Lett. 94,102301 (2005); 96, 039901(E) (2006).
96 [2] L. Adamczyk et al., (STAR Collaboration), Nature 548, 62 (2017).
97 [3] I. Karpenko and F. Becattini, Eur. Phys.J. C 77, 213 (2017).
98 [4] J. Adam et al., (STAR Collaboration), Phys. Rev. C 98, 014910 (2018).
99 [5] S. Alzhrani, S. Ryu, and C. Shen, Phys. Rev. C 106, 014905 (2022).
100 [6] B. C. Fu, et al., Phys. Rev. Lett. 127, 142301 (2021).
101 [7] J. Adam et al., (STAR Collaboration), Phys. Rev. Lett. 123, 132301(2019)
102 [8] S. Acharya et al., (ALICE Collaboration), arXiv:2107.11183.